

UC Berkeley

UC Berkeley Previously Published Works

Title

Coupling covariance matrix adaptation with continuum modeling for determination of kinetic parameters associated with electrochemical CO₂ reduction

Permalink

<https://escholarship.org/uc/item/4pv479p5>

Journal

Joule, 7(6)

ISSN

2542-4351

Authors

Corpus, Kaitlin Rae M

Bui, Justin C

Limaye, Aditya M

et al.

Publication Date

2023-06-01

DOI

10.1016/j.joule.2023.05.007

Copyright Information

This work is made available under the terms of a Creative Commons Attribution-NonCommercial-NoDerivatives License, available at

<https://creativecommons.org/licenses/by-nc-nd/4.0/>

Peer reviewed

Coupling Covariance Matrix Adaptation with Continuum Modeling for Determination of Kinetic Parameters Associated with Electrochemical CO₂ Reduction

Kaitlin Rae M. Corpus^{1,2‡}, Justin C. Bui^{1,2‡}, Aditya M. Limaye³, Lalit M. Pant^{4,5}, Karthish Manthiram^{6,7}, Adam Z. Weber^{2,4}, & Alexis T. Bell^{1,2*}

¹Department of Chemical and Biomolecular Engineering
University of California Berkeley
Berkeley, CA 94720, USA

²Liquid Sunlight Alliance
Lawrence Berkeley National Laboratory
Berkeley, CA 94720, USA

³Department of Chemical Engineering
Massachusetts Institute of Technology
Cambridge, MA 02139, USA

⁴Energy Technologies Area
Lawrence Berkeley National Laboratory
Berkeley, CA 94720, USA

⁵Department of Sustainable Energy Engineering
Indian Institute of Technology, Kanpur
Kanpur, UP-208016, India

⁶Division of Chemistry and Chemical Engineering
California Institute of Technology
Pasadena, CA 91125, USA

⁷Liquid Sunlight Alliance
California Institute of Technology
Pasadena, CA 91125, USA

Corresponding Author and Lead Contact: alexbell@berkeley.edu
Phone: (510)-642-1536

[‡]Contributed equally

Summary (150 words)

In electrocatalysis, the rate of a reaction as a function of applied potential is governed by the Tafel equation, which depends on two parameters: the Tafel slope and the exchange current density (i_0). However, current methods to determine these parameters involve subjective removal of data due to the convoluted effects of mass transfer and competitive surface or bulk reactions, resulting in unquantifiable uncertainty. To overcome this challenge, we couple covariance matrix adaptation with a continuum model of CO₂ reduction (CO₂R) that explicitly deconvolutes non-kinetic effects to extract kinetic parameters associated with 27 literature datasets of CO₂R over Ag and Sn catalysts. The fitted kinetic parameters do not converge to a unique set of values, and the Tafel slope and i_0 possess an apparent correlation, which we suggest is a consequence of variations in catalyst preparation methods. This work facilitates rigorous benchmarking of electrocatalysts in systems where mass transfer is relevant.

Introduction

Electrochemical reduction of CO₂ (CO₂R) emitted from point sources (e.g., cement production, separation from natural gas, iron and aluminum ore smelting, and fermentation of sugars) using electricity from renewable resources (e.g., wind and solar) offers a means for recapturing its carbon content. Moreover, if the CO₂ can be taken from the atmosphere and converted electrochemically to chemicals and fuels, one could envision a closed carbon cycle.¹⁻⁴ In order to produce desired products with high rates and selectivity, it is important to understand how to design electrochemical cells that enable achievement of these objectives.⁵⁻⁸ A key element in pursuit of this goal is accurate representation of individual product formation rates and their dependence on reactant concentration, pH, and cathode potential.

For the design and simulation of electrochemical processes, the current density (i_j) for producing product j is most commonly based on the Butler-Volmer equation (Equation (1)) or the simpler Tafel equation (Equation (2)), which is based on the assumption that the reaction is irreversible at large overpotentials. In this work we only consider the Tafel equation for the cathodic direction.

$$i_j = i_{0,j} \left(-\exp\left(\frac{-\alpha_{c,j}F}{RT} \eta_j\right) + \exp\left(\frac{\alpha_{a,j}F}{RT} \eta_j\right) \right) \quad (1)$$

$$i_j = -i_{0,j} \exp\left(\frac{-\alpha_{c,j}F}{RT} \eta_j\right) \quad (2)$$

Here R is the ideal gas constant, F is Faraday's constant, η_j is the overpotential or driving force for the electrochemical reaction j , T is the absolute temperature, $\alpha_{c,j}$ is the transfer coefficient, and $i_{0,j}$ is the exchange current density. In Equation (2), there are two important parameters, the transfer coefficient ($\alpha_{c,j}$) that describes the sensitivity of the product current density to changes in the overpotential (*i.e.*, the electrochemical driving force) and the exchange current density ($i_{0,j}$), which is the pre-factor for the exponential term.⁹ It is important to note that the exchange current density contains explicit concentration dependences on the reactants and products of a given reaction, as derived in **Supplemental Note S1**.

Many studies of electrochemical synthesis report the Tafel slope, which is directly related to the transfer coefficient defined as the overpotential required to obtain a ten-fold increase in product current density.^{9,10}

$$\text{Tafel Slope} = \frac{-\ln(10)RT}{\alpha_{c,j}F} = \frac{-59.125 [mV \text{ dec}^{-1}]}{\alpha_{c,j}} \text{ for } T = 298 \text{ K} \quad (3)$$

For multi-step kinetics, the Tafel slope, or related the transfer coefficient $\alpha_{c,j}$, has been used to infer which elementary step is rate-limiting in the formation of a particular reaction product.¹¹⁻¹³

A commonly used method to calculate Tafel slopes involves a least-squares regression on the linear portion of the logarithm of the measured current density vs cathode potential (i.e., the kinetic region of the polarization curve). This approach involves manual exclusion of data that lie in the mass-transport limited regime (Figure 1, **top**).¹⁰ For the electrochemical reduction of CO₂, the mass-transport-limited regime occurs at potentials for which the predicted rate of CO₂ consumption by electrochemical and homogeneous chemical reactions becomes greater than the rate of CO₂ transport to the surface. Mass-transport limitations in CO₂R are caused primarily by the low solubility and diffusion coefficient of CO₂ in the aqueous electrolyte.^{14,15} Because the regimes of kinetic control and the onset of mass-transfer control are defined arbitrarily, this method of identifying the regime of kinetic control is prone to human error and leads to a reduction in the number of data points available for analysis. It is also notable that in electrochemical synthesis the product must be quantified at every applied potential through time-consuming steady-state measurements. The need for product quantification contrasts with water electrolysis for which catalytic behavior can be measured rapidly at thousands of points via linear-sweep voltammetry. Because data in electrochemical synthesis must be collected by steady-state chronopotentiometry or chronoamperometry to generate sufficient product for quantification, rapid current-voltage sweeps are impractical if one wants to determine the partial current densities for each product. In other words, the steady-state nature of electrochemical synthesis, in which multiple products are formed, limits the number of available data points for each product.

Prior work has sought to address these concerns and provide rigorous methods for determining kinetic parameters.^{10,16,17} Recently, Limaye *et al.* have attempted to address the challenge of data insufficiency in Tafel analysis for electrochemical CO₂R by using a Bayesian learning algorithm,¹⁰ in which current-voltage data are fit to a representation of the intrinsic reaction rate given by the Tafel equation together with the effects of mass transfer. Using such a model enabled fitting of all experimental data without the need to arbitrarily define the Tafel region, even for limited data sets (5-20 data points). Furthermore, the Bayesian learning model used in this work provided a distribution of potential Tafel slopes and a defined uncertainty threshold. This approach revealed the human errors in involved fitting Tafel slopes reported in the literature. A limitation of this work is that the physical model employed did not account for coupling of mass transfer effects with competing electrochemical and homogeneous buffer reactions that consume reactants and change local pH,¹⁸⁻²⁰ as well as the complex dependences of the intrinsic kinetics on species activities that affect observed kinetics,^{6,19,21,22} preventing the approach from capturing complex curvature in the CO₂R polarization curve at higher applied potentials or deconvoluting of contributions due to various surface reactions.

In this work, we present a one-dimensional, reaction-transport model of the CO₂R to CO and H₂ over Ag catalyst, as well as CO₂R to HCOOH, CO, and H₂ over an Sn catalyst, that is then used in combination with covariance matrix adaptation evolutionary strategy (CMA-ES), an advanced data analysis tool, to fit the Tafel parameters (i.e., α_c and i_0) for a variety of Ag and Sn catalysts. This approach provides a rigorous means for identifying the parameters required for continuum simulations without the need for subjective human intervention while accounting for mass transfer, which sensitivity analysis elucidates is key to accurately determining kinetic parameters. Application of this approach to 18 data sets for CO₂R to CO on Ag, as well as 8 data sets for CO₂R to CO and HCOOH on Sn, in similar experimental setups reveals that the fitted rate parameters are broadly distributed, probably due to differences in catalyst morphology (*i.e.*, distribution of surface facets and roughness) that we propose

could be a result of variations in catalyst preparation across various studies. The methodology reported here provides a rigorous approach for determining the Tafel parameters associated with product partial current density vs. cathodic potential curves obtained for electrochemical processes that produce multiple products. This finding is particularly important for systems in which the formation of one product influences the rate of formation of other products through the effects of mass transfer and bulk reactions.

Results and Discussion

Continuum Modeling to Assess Traditional Tafel Fitting

To assess the impact of mass transport and bulk reactions on observed partial current densities, a sensitivity analysis was carried out. By this means, the sensitivity of the product partial current densities to changes in the kinetic parameters ($\alpha_{i,c}$ and $i_{i,0}$) is determined. (**Supplemental Note S2**) This procedure enables an assessment of the degree of sensitivity between the outputs and input parameters in the model (*i.e.*, how much an output parameter changes when an input parameter is changed). When an output is positively sensitive to an input, an increase in the input results in an increase in the output; when an output is negatively sensitive to an input, an increase in the input results in a decrease in the output. The sensitivity analysis revealed that the CO partial current density is highly negatively sensitive to mass transfer (*i.e.*, L_{BL}) due to low availability of CO₂ in the aqueous electrolyte; however, the H₂ partial current density is less sensitive to mass-transfer effects because of the high availability of solvent water, which was assumed to be the proton source for HER. (**Figures S3-5**) We also observed that the CO partial current density was positively sensitive to $i_{0,CO}$ and α_{CO} , but more interestingly, negatively sensitive to the HER kinetics (i_{0,H_2} and α_{H_2}) (**Figure S3**). As the HER current increases, the pH rises due to concomitant generation of OH⁻, and the generated OH⁻ anions consume reactant CO₂ via homogeneous buffer reactions thereby reducing the COER partial current.

Continuum simulations were then used to assess the accuracy of the traditional Tafel analysis (see **Section S5, Supplemental Note S3**) for simulated polarization curves where mass transport or

competitive reactions were relevant. Figure 2**a-b** depict the results of performing traditional Tafel analysis to extract the kinetic parameters from CO polarization curves generated by the simulation, all of which possess a constant CO Tafel slope but different values of L_{BL} (Figure 2**a**) or i_{0,H_2} (Figure 2**b**). In other words, these plots possess a constant value of the intrinsic kinetic parameters of COER ($i_{0,CO}$ and $\alpha_{c,CO}$), but the value of L_{BL} is changed from $0.5\times$ to $1.5\times$ its base value (Figure 2**a**), and the value of i_{0,H_2} is changed from $1\times$ to $100\times$ its base value (Figure 2**b**). As can easily be seen, even though the CO Tafel slope should be identical for all plotted polarization curves, the apparent Tafel slope as measured by a traditional approach is different for every curve, revealing the extent to which mass transport affects the apparent Tafel slope. Key to this sensitivity analysis is the recognition that concentration gradients in CO_2 and pH within the mass-transport boundary layer are quite severe (Figure S6), particularly at high potentials, meaning that the concentration in the bulk is not the same as the concentration at the reaction plane, and that the large gradients in reactant activity within the boundary layer necessitate the simulation of mass transport to determine activities accurately at the reaction plane. Therefore, the continuum model is necessary to deconvolute the effects of mass transport from the intrinsic kinetics of the surface reactions.

Intriguingly, when the apparent CO Tafel slope (Figure 2**c**) and $i_{0,CO}$ (Figure S7) are plotted against L_{BL} , they approach their intrinsic values as L_{BL} approaches zero. In other words, in the limit of no mass-transport losses of CO_2 , traditional Tafel fitting is sufficient and accurate. This finding suggests traditional assessment of Tafel slopes could be done using data that are minimally affected by mass transfer. Porous electrodes, which have boundary-layer thicknesses approaching the nanometer length scale, have also been suggested for determining the intrinsic kinetics of electrochemical reactions.^{3,39} However, the chemistry and morphology of such electrodes were found to impact observed kinetics in non-trivial ways due to the potential of overlapping boundary layers, along with the complex multiphase (gas, liquid, and sometimes solid-electrolyte phases) transport occurring in the porous medium.³ Rotating

disk³⁵ or rotating cylinder^{40,41} electrode systems can also aid in deconvoluting the effects of mass transfer. However, the use of these techniques does not eliminate completely mass transfer at high cathode potentials and current densities. Therefore, modeling of mass transport and the kinetics of bulk reaction occurring in an aqueous boundary layer (see below) will always be necessary for determination of Tafel parameters.

In addition to hydrodynamics, the presence of bulk reactions occurring in the thin boundary layer can impact the apparent Tafel slopes. Figure 2b and S9 illustrate the effect of the HER current density on apparent CO kinetics, demonstrating that at high current densities for HER, the apparent CO kinetic parameters can be quite inaccurate. However, this competition for reactant CO₂ is indirect and is a result of consumption of HER-generated OH⁻ anions to form HCO₃⁻ and CO₃²⁻ anions in the boundary layer, as opposed to direct electrochemical consumption. Indeed, many catalysts experience direct electrochemical competition for reactant CO₂. For instance, formate (HCOO⁻) forms competitively with CO on Cu,⁸ Pd,⁴² Sn⁴³⁻⁴⁵, and Ag,²⁴ and such direct competition for CO₂ impacts the apparent Tafel slopes for these products. As shown in Figure 2d, the occurrence of competing HCOO⁻ formation dramatically increases the apparent CO Tafel slope beyond its intrinsic value. For the largest $i_{0,HCOO^{-}}$ tested, corresponding to roughly equal co-generation of CO and HCOO⁻, as has been observed on Cu⁸ and Pd⁴², the CO Tafel slope is nearly 50 mV dec⁻¹ larger than the reference value employed in the model (93.55 mV dec⁻¹). $i_{0,CO}$, $\alpha_{HCOO^{-}}$, and $i_{0,HCOO^{-}}$ exhibit similar inaccuracies. (**Supplemental Note S3**)

The transfer coefficient quantifies how much of the applied potential driving force goes to driving the rate of a given electrochemical reaction. In electrochemical synthesis systems, the applied potential driving force drives a suite of competitive surface reactions and overcomes losses attributable to low rates of mass transfer (*i.e.*, Nernstian losses). Thus, taking kinetic parameters directly from measured polarization data typically leads to an overestimation of the Tafel slope (and, hence, an underestimation of the transfer coefficient due to their inverse proportionality) by neglecting the potential losses associated

with mass transport and competitive surface reactions. As mass transfer improves, and in the limit of a single surface reaction, the intrinsic kinetics can be measured experimentally. However, the presence of competing electrochemical reactions and poor mass transfer is the norm in electrochemical synthesis, rather than the exception. These results underscore the need for physiochemical models that enable determining the intrinsic Tafel parameters for individual reaction kinetics unaffected by the effects of mass transport, bulk reactions occurring the mass-transfer boundary layer, or competing surface reactions.

Recent work has attempted to delineate more accurately the kinetically controlled and mass transport controlled regimes in polarization data by employing a technique known as differential Tafel analysis, in which Tafel slopes and/or their derivatives are plotted as a function of potential.^{46,48} However, differential Tafel analysis requires substantial data collection and is quite challenging for electrochemical synthesis application, for which product quantification as a functional of potential, particularly liquid-phase products, limits data availability. Even if data insufficiency were not a concern, differential Tafel analyses would not be able to fully deconvolute the contributions to partial current density from mass transport and kinetics due to the significant impact of mass transfer in these CO₂ reduction reactions at nearly all relevant applied potentials (**Supplemental Note S4**). This is especially true for minority products such as HCOO⁻ on Ag, for which there are no regions in which differential Tafel analysis can identify kinetic control. By accounting for mass transfer effects directly in the mathematical model, the method reported here enables direct simulation of the various competing phenomena and, correspondingly, the extraction of kinetically relevant Tafel parameters for multiple surface reactions simultaneously for CO₂ reduction.

Fitted Tafel Parameters

Having established that our model and approach for fitting Tafel parameters is capable of simultaneously fitting the parameters for CO and H₂ formation for different sets of data taken from the literature with high accuracy and quantified uncertainty without human intervention (see **Section S7** for

plots of all H₂ and CO polarization curves and the corresponding fitted Tafel parameter values), we sought to determine whether the fitted Tafel slopes and transfer coefficients converged to a set of unifying values. Bockris and co-workers derived what they refer to as cardinal values for the transfer coefficient of $\alpha_c = \dot{i}$ 0.5, 1.0, 1.5, *etc.*¹³ This can be done starting with **Equation S62** and assuming integer values for s and q , a ν of 1, and a symmetry factor of the rate determining step, $\beta = 0.5$. Correspondingly, cardinal values for the Tafel slope (**Equation S40**) are 118, 59, 39, *etc.* Crucially, the symmetry factor, which is defined as the fraction of the applied overpotential that goes towards lowering the barrier of the cathodic reaction (as opposed to the anodic reaction),⁴⁹ will likely not be 0.5 for inner sphere electrochemical reactions such as CO₂R and HER on Ag, where some potential is lost in the double layer,³ and the reaction intermediate is likely not equidistant in free energy from the reactants or products.⁴⁷ Nonetheless, many theoretical studies have employed the cardinal value of 0.5 for CO₂R.^{10,50,51} It is also notable that the theoretical work of Singh *et al.* employs density functional theory (DFT) and finds an effective cathodic transfer coefficient of 0.49.⁴⁷ They also find transfer coefficients of 0.23 and 0.05 for the Volmer and Heyrovsky steps, respectively, where the latter is rate limiting.⁴⁷ Due to the effects of surface roughness on the exchange current density, there are no “cardinal values” for the exchange current density; i_0 is expected to vary drastically based on the morphology of a given electrode.

Figure 3 illustrates the probability distribution functions (PDFs) and kernel density estimates (KDEs) for **(a)** α_{CO} , **(b)** $\log_{10}(i_{0,CO})$, **(c)** α_{H_2} , and **(d)** $\log_{10}(i_{0,H_2})$. These plots show that these parameters do not converge to a single set of values, as further demonstrated by the cumulative distribution functions shown in **Figure S10**. The fitted parameter distributions for the Tafel slopes and boundary-layer thicknesses are given in **Figures S11** and **S12**. It is important to note that all fitted parameters lie within a range of physically acceptable values, and possess a tighter range than those previously reported for continuum models.³ Interestingly, the most probable values of the transfer coefficients for both CO and H₂ (determined as the maxima of the KDEs (see **Table S12**)) are quite far from the so-called “cardinal

values”, but lie relatively close to the values reported by Singh *et al.* that were obtained via DFT of CO₂R and HER on Ag (110) (difference of 0.10 for α_{CO} , difference of 0.04 for the Volmer step α_{H_2}).⁴⁷ However, this could just be coincidental, and greater effort should be employed to bridge the results observed in continuum level and *ab-initio* level models.

Additionally, consistent with the analysis above, we demonstrate that accounting for mass transfer helps mitigate the overprediction of Tafel slopes, shifting the distribution towards lower values when mass transfer is explicitly handled (**Figure S13**). It is important to note that the size of the data set could simply be too small to observe a sharp distribution in the fit parameters due to small variabilities or errors in the experimental measurements. Collecting more data in similar conditions could potentially lead to the distribution better predicting theoretically expected values. Nonetheless, the broad distribution of parameters makes it impossible to prescribe a unique set of values that are descriptive of the CO₂R on all Ag catalysts and indicate that Tafel parameters need be fitted for each individual Ag catalyst.

To address the spread of values in the fitted parameters, we note that the transfer coefficient itself may be a function of the applied potential as predicted by Marcus theory,¹⁷ because at negative potential, the transition state is more initial-state like ($\beta_{RDS} \rightarrow 0$) and at positive potential the transition state is more final-state like ($\beta_{RDS} \rightarrow 1$).⁵² However, Marcus inversion is not expected to be significant over the relatively small potential ranges studied experimentally, and all of the studies used were performed with nearly identical potential ranges. Thus, Marcus theory is unlikely to explain the spread in fitted parameters, and it is more likely that the observed spread in values is due to differences in surface morphology among different samples of Ag cathodes. The presence of a bicarbonate reduction pathway could also explain some of the observed spread in parameters. We sought to determine if there were any effects of bicarbonate concentration on the fit kinetics for HER, potentially due to proton donor effects. Notably, when we plot the fit kinetic parameters for HER as a function of the bulk electrolyte concentration (**Figure S16**), we observe no clear trend in the fit kinetic parameters with respect to bicarbonate

concentration, suggesting that the bicarbonate concentration does not have a direct impact on the observed HER kinetic parameters.

We also compared the HER kinetic parameters taken from analyzing data obtained during CO₂R on Ag catalysts to those obtained from an analysis of HER data acquired for polycrystalline Ag in 0.1 M KHCO₃ under an N₂ atmosphere²³, as discussed in **Supplemental Note S6**. The fitted transfer coefficient for the HER ($\alpha_{c,H_2}=0.199$) acquired in the absence of dissolved CO₂ is nearly identical to the most probable value ($\alpha_{c,H_2,MP}=0.195$) calculated with CO₂R data. The exchange current density without CO₂ ($i_{0,H_2}=10^{-3.16} \text{ mA cm}^{-2}$) is also comparable to that obtained from the most probable value of the parameter distribution ($i_{0,H_2,MP}=10^{-2.49} [\text{mA cm}^{-2}]$) from an analysis of the data for CO₂R.

Ultimately, we contend that differences in catalyst preparation for the studies examined are the primary cause for the broad distributions observed (**See Table S10** for a detailed description of the preparation methods). Indeed, surface roughness is expected to contribute to the spread in fitted exchange current densities, as the roughness factor is implicitly lumped into that parameter (**Equation S79**).³ The Ag catalysts used in the studies we have examined are typically polycrystalline. Clark *et al.* have shown that different Ag facets on polycrystalline Ag possess different intrinsic activities for CO₂R (**Figure S14**).²⁶ More recently, Gauthier *et al.* have demonstrated that surface preparation and roughening affect the intrinsic activity of a given catalyst for CO₂R.⁵³ Therefore, the spread in transfer coefficient (and thus Tafel slope) could reflect the changes in the distribution of surface structuring for different catalysts. Differences in surface coverage by poisons may also impact the observed kinetic parameters.⁵⁴

Compensation Effects in Electrocatalytic CO₂R on Ag

An important question is whether the transfer coefficients, exchange current densities, and the boundary-layer thickness (α_{c,H_2} , $\alpha_{c,CO}$, i_{0,H_2} , $i_{0,CO}$, and L_{BL}) are correlated with each other. We first sought to assess whether the bulk electrolyte concentration and the boundary-layer thickness are

correlated with the fitted transfer coefficients and exchange current densities, which should be intrinsic to the catalyst. **Figures S15-S16** confirm that the lack of correlation between these parameters for all the fitted data. We next explored the correlation between the fitted values of α_c and i_0 for each reaction. The parameters α_c and $\log_{10}(i_0)$ should exhibit a negative, linear correlation with the slope of the correlation line related to the reaction order of the reactant and product species and their activity in the bulk electrolyte because the expression for i_0 is referenced to the activities of species in the bulk electrolyte (**Supplemental Note S7**). While a negative correlation is observed for both reactions (Figure 4), the slopes are much more negative than would be expected from the derivation in **Supplemental Note S7**. Additionally, these data were carried out using different bulk electrolyte concentrations and Ag electrodes having different roughness factors. As can be seen in **Equation S89** both factors impact the exchange current density. These effects are not explicitly deconvoluted from the correlation observed in Figure 4 (roughness factors are seldom reported), so one should not expect any correlation in the plotted data. Vetter performed traditional Tafel analysis on various HER catalysts and demonstrated that while α_{H_2} was somewhat consistent across all tested catalysts, the $\log_{10}(i_{0,H_2})$ varied across these catalysts varied by many orders of magnitude and were uncorrelated with α_{H_2} .^{9,55} Therefore, the apparent correlation between the fit α_c and $\log_{10}(i_0)$ is unexplained.

We note that a correlation has been observed in thermal catalysis between the pre-exponential factor and the activation energy, and is referred to as the “compensation effect”.⁵⁶⁻⁶⁰ Barrie has discussed the mathematical origins of this effect and its relationship to random experimental errors.⁶⁰ In this connection, Bond *et al.* have proposed a set of guidelines to establish when the effect is physically meaningful.⁵⁷ First, the dataset of interest must be sufficiently large; the range of transfer coefficients should be such that the largest value is at least 50% greater than the smallest. Second, the effects of the reaction order and bulk species concentration must be properly accounted for (**Figure S17**). Lastly, we add that, for electrocatalysis, the effects of active surface area should be properly deconvoluted. For the

data fit in this work, experiments were all reported based on geometric surface area of the cathode rather than the electrochemically active surface area (ECSA), making roughness effects difficult to deconvolute. Lastly, to account for any effects of bicarbonate rate order, we also explicitly color-code the compensation plots by bicarbonate concentration, showing that the compensation phenomenon still exists when accounting for differences in bulk bicarbonate concentration (**Figure S18**).

All considered, the existence of an apparent correlation likely suggests that, among other factors, a lack of standardization in catalyst preparation leads to apparent compensation effects that contribute to the broad distribution of the fitted parameters observed above. Future work should use more sophisticated objective functions that weigh data points according to their associated uncertainty, but the underlying issue is that many reports in CO₂R do not report sufficient polarization data with defined error bars. Additionally, reporting electrochemical data with respect to ECSA or using less-complex electrodes would also improve data quality for model fitting by deconvoluting the effects of surface roughness from the exchange current density, better enabling analysis of apparent compensation phenomena. Indeed, the need for more easily interpretable electrocatalytic measurements has been well-documented in recent work.⁶¹ Lastly, recent studies have demonstrated the impact of forced convection on observed Tafel slopes.⁶² Correspondingly, future work should aim to implement the developed method with rotating disk electrode experiments and a rigorous continuum model of a rotating disk electrode to validate continuum theory over multiple regimes of mass transport and explore the effects of forced convection on observed kinetics. The analysis presented here further underscores the need for better standards and protocols for acquisition of experimental data that can then be used to validate results obtained by theoreticians.

Extension of Method for Analysis of CO₂R over Sn Catalysts

To demonstrate the extension of the developed method to more complex electrochemical synthesis systems, the coupled CMA-ES continuum modeling approach was applied to 8 additional datasets of

CO₂R over Sn catalysts acquired in H-cells. Sn catalysts add complexity compared to Ag because they additionally generate HCOO⁻ along with CO and H₂. However, similar to Ag, they weakly bind CO and H, so explicit adsorbate coverage effects are still negligible.⁸ To enable fitting of these data, the continuum model was updated to capture the physics related to HCOO⁻ formation. As shown in **Figure S19**, our method is highly capable of determining kinetic parameters and can reproduce experimental data simultaneously for CO, H₂, and HCOO⁻ over Sn with high accuracy and quantified uncertainty.

The distribution of kinetic parameters shown in Figure 5 for Sn are similarly broad to those collected on Ag, again likely due to large variations in catalyst preparation used by different investigators (**Table S21**). Interestingly, the distribution of fitted HER kinetic parameters looks like that for Ag, suggesting that HER on Sn occurs through a similar pathway on Sn and Ag. Conversely, the distribution of fitted parameters for CO formed on Sn and Ag looks quite different, suggesting different mechanistic pathways or energetics for CO on the two metals.

Future work should implement the effects of adsorbate coverages into the continuum model to assess more complex CO₂R catalysts where intermediate binding is important and variable, such as Cu. To do so requires the use of microkinetic models of CO₂R that are validated by independent spectroscopic data. We also note that the present approach is not limited to CO₂R but should be applicable to for other electrochemical reactions, such as carboxylation⁶³, epoxidation⁶⁴, and ammonia synthesis.⁶⁵

Conclusions

The present study describes a method for fitting Tafel parameters for multiple reactions occurring during the electrochemical reduction of CO₂ over Ag catalysts. This approach combines continuum modeling and advanced data-science methods (covariance matrix adaptation-evolutionary strategy (CMA-ES)) to fit the parameters appearing in the Tafel equations used to describe the kinetics of CO and H₂ formation. The method developed here avoids unquantifiable uncertainty associated with the subjective demarcation between the portions of the product polarization curves associated purely with reaction kinetics and that convoluted with the effects of mass transfer and buffer reactions. A continuum model is employed to account for mass transport and bulk-phase homogeneous buffer reactions. We show that neglecting these phenomena leads to systematic overprediction of the Tafel slope and exchange current density obtained using traditional methods of analysis.

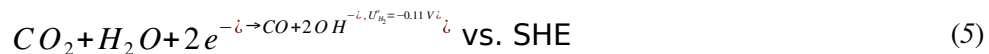
The coupled CMA-ES continuum modeling approach is applied to 18 data sets for CO₂R on Ag, obtained in similar electrochemical cells and using KHCO₃ as the electrolyte, to determine rate parameters for CO₂R to CO and H₂, and a broad distribution of fitted Tafel parameters is observed. The distribution of values of the transfer coefficient and the exchange current density are attributed to differences in the structure and morphology of different Ag catalysts due to differences in catalyst preparation methods used by various authors. Lastly, we show that our method of data analysis can easily be adapted to more complex reaction systems by employing the method to perform a similar analysis of the kinetic parameters for CO₂R on Sn catalyst, which produces HCOO⁻ along with CO and H₂. The Tafel parameters for Sn were broadly distributed in a manner like those for Ag. Ultimately, this work demonstrates and quantifies the need to account for the effects of mass transfer and buffer kinetics in the analysis of product partial current densities obtained for the electrochemical reduction of CO₂.

Experimental Procedures

Continuum Model

Figure 6Error: Reference source not found illustrates the one-dimensional (1-D) model used to simulate mass transport and reaction occurring in an electrochemical cell performing CO₂R. The modeled domain consists of a planar Ag electrode, an aqueous potassium bicarbonate (KHCO₃) electrolyte, and the associated mass-transport boundary layer. The bulk concentration of the KHCO₃ electrolyte is chosen to coincide with that used in the experimental data set to be fitted, and the thickness of the associated mass-transport boundary layer (L_{BL}) is fit along with the kinetic parameters. We note further that all of the experimental data examined in this study were acquired using a flow cell (*i.e.*, an) with well-defined hydrodynamics and a reference electrode located in the potassium bicarbonate electrolyte (Figure 6Error: Reference source not founda).^{23–32} The decision to consider only Ag or Sn catalysts used under similar experimental conditions limits the amount of available data in literature but enables deconvolution of the catalytic behavior from other variables. Additionally, we choose these catalysts because they bind CO and H weakly.⁸ This justifies the assumption of near unity empty site coverage invoked when using a global Butler Volmer or Tafel kinetic rate law, as is done here.¹² Additionally, any effects of coverage will be embedded in the fit values for the parameters obtained. To extend this method to catalysts such as Cu that bind CO or H stronger requires explicit consideration of coverage effects. We note that previous work has shown that a 1-D representation is capable of capturing the requisite concentration and potential gradients needed to model aqueous CO₂R on planar catalysts.^{14,33,34}

The CO and H₂ evolution reactions (COER and HER) occur at the surface of the Ag electrode, with the following stoichiometries and standard potentials.



A concentration dependent Tafel expression was used for each product to model the kinetics of the competing reactions (for which the kinetic parameters will be fit),

$$i_{CO} = \left(\frac{a_{CO_2}}{a_{CO_2}^{bulk}} \right)^{-\gamma_{c,co}} i_0 \quad (6)$$

$$i_{H_2} = i_0 \quad (7)$$

where $i_{0,j}$ and $a_{c,j}$ are the exchange current density and cathodic transfer coefficient for product j , respectively. These parameters are obtained by our fitting method described in the **Experimental Procedures**. $\gamma_{i,j}$ represents the rate order of species i in the reaction to form species j and is constrained by its relationships to the transfer coefficients, as given by **Equations S10-14**. It is important to note that the effects of the electrolyte cation, which are important for COER kinetics, will be implicitly captured by the fit exchange current density (**Equation S79**),³⁵ given the fact that all data considered in this work employ the same electrolyte cation (K^+). Additionally, recent work has suggested that the reduction of bicarbonate to form H_2 could also contribute to HER current density.^{23,36} However, the extent to which the proton donor dictates HER is still up to substantial debate, with most works only attributing a small current density feature at moderate applied potentials to bicarbonate reduction.²³ These studies suggest that H_2O will likely be the dominant proton donor at all applied potentials relevant to CO_2R .²³ Therefore, for simplicity, we only consider water as a proton donor.

In the above expressions, a_i represents the activity of species i locally at the electrode surface, as calculated by the reaction-transport simulation, and a_i^{bulk} represents the activity of species i in the bulk electrolyte. Activities are used as the driving force for both electrochemical reactions (**Section S1.2**) and homogeneous bulk reactions occurring within the boundary layer (**Section S1.3**). These activities are determined by accounting for the excess chemical potential due to long- and short-range electrostatics through the Davies activity coefficient model for ionic species. Changes to the CO_2 solubility due to species-species interactions are accounted for through the Sechenov activity coefficient model for CO_2 (**Section S1.2**). The terms involving the ratio of the surface and bulk activity account for mass-transport and concentration gradients within the boundary layer (**Section S4**). $\eta_{s,i}$ is the surface overpotential for a given electrochemical reaction defined in **Equations S19-S21** in the **SI**. Ultimately, the inclusion of these

effects allows for the accurate calculation of species activities at the reaction plane for CO₂R, which determine the rates of the electrochemical reactions occurring at the electrode surface. A detailed description of the physics employed in the model, as well as a generalized derivation of the kinetic model, can be found in the **Supplemental Experimental Procedures**.

Covariance Matrix Adaptation Evolution Strategy

To minimize the objective function, which in this case is the mean square error (MSE) of the fit to the CO and H₂ specific polarization curves, the covariance matrix adaptation evolutionary strategy (CMA-ES) was employed (shown schematically in Figure 7). CMA-ES is a global, derivative-free optimization method that operates by forming a parametric distribution over the solution space. It samples a population of solution candidates iteratively, typically from a multivariate gaussian distribution.³⁷ This objective function is then evaluated for each candidate set of parameters. After evaluating the objective function for each point in each generation of solution candidates, the solutions are sorted by the magnitude of the objective function and the distribution parameters (the mean vector and covariance matrix) are updated based on the ranking of objective function values. The goal is to search for the optimum set of parameters, such that the objective function is a minimum. The method stops once the change in error across generations has dropped below a certain tolerance (in this study, a tolerance of 1×10^{-11} was used, which is the default in CMA-ES algorithm in MATLAB.) It is critical to note that CMA-ES is gradient-free since the objective function used for fitting the Tafel kinetic is non-convex, so there exist many local minima in which a gradient-descent method can get trapped. Notably, previous work has shown that small changes in the fitted Tafel parameters can lead to local minima that approximately fit experimental data.¹⁷ We also note (**Section S1.9**) that using a gradient-descent method (e.g., MATLAB's `fmincon`) in lieu of the CMA-ES method ultimately fails to fit experimental polarization data (**Section S6**).

Description of Fitting Method

The process shown schematically in Figure 8 was used to fit the experimental data. First, the reported cathode potentials (usually referenced to a reversible hydrogen electrode (RHE)) were shifted to the standard hydrogen electrode (SHE) potential, by (see Figure 8b):

$$\phi_c[V \text{ vs. } SHE] = \phi_c[V \text{ vs. } RHE] - 0.059 \times pH_{bulk} \quad (8)$$

This change of reference makes the experimentally measured potentials consistent with the potentials used in the model (**Sections S1.1-1.3**).

Next, the parameters for each reaction were fitted one reaction at a time in order to separate the $((2k \times 2k) + 1)$ dimensional optimization problem (where k is the number of competing reactions and the $+ 1$ is due to fitting L_{BL}) into $(k - 1)$ 2-dimensional optimizations and a single 3-dimensional optimization (in which the thickness of the boundary layer is fit). This procedure makes the problem more tractable and avoids the so-called ‘‘curse of dimensionality’’ in optimizations.³⁷ It is also important to note that fitting the boundary layer was necessary to provide the best fit for the CO data, as the boundary-layer thickness dictates the mass-transport-limiting plateau (see **Figure S2**), and is seldom measured or reported for CO₂R current densities measured using a flow cell. We note that the fitted mass-transport boundary-layer thicknesses generally agree in terms of order of magnitude with values reported in previous flow cell studies;^{15,38} any discrepancies are likely due to assumed Sherwood relationships for the calculation of the mass-transfer coefficient, which, in most cases, do not account for the effects of homogeneous buffer reactions and multi-ion transport.¹⁵ Additionally, these boundary layer thicknesses also vary quite substantially with cell design.^{15,38} For all the reasons noted, we choose to fit the apparent or effective boundary-layer thickness (L_{BL}) as an adjustable parameter.

To fit the kinetics for CO formation, the reference-shifted experimental data for H₂ partial current density versus voltage are imported into the CMA-ES algorithm and are held fixed. Doing so is critical for calculating the kinetic parameters for CO formation because H₂ data enable the model to calculate

changes in the local pH and CO₂ concentration that result from HER, which, in turn, affect kinetics of CO formation. The initial guesses for fitting are shown in **Figure S1**. The COER current density is defined by Equation (6). The CMA-ES algorithm then uses the transport and reaction model to obtain the best values of $\alpha_{c,CO}$, $i_{0,CO}$, and L_{BL} that give the best fit to the data (Figure 8c). Once the CO kinetic parameters and L_{BL} are determined, they are fixed to their fitted values and the parameter for the HER partial current, α_{H_2} and i_{0,H_2} , described by Equation (7) are fitted using the CMA-ES algorithm (Figure 8d). Post processing of the CMA-ES distributions provides the uncertainty. This process can be easily generalized to a system containing a greater number of competing reactions as described in **Sections S1.10-1.11**. While this overall process could be repeated to further reduce error, doing so results in only a minor change in the fitted parameters (< 0.1% change in α , < 0.2% change in L_{BL} , and < 0.7% change in i_0) and comes at greater computational expense. Thus, for this work, the fitting process was run once through each product. When fitting for Sn, because HCOO⁻ was the major product, HCOO⁻ was fit first, followed by CO, and lastly finishing the fitting process with H₂ (**Section S1.10**). This process could be similarly generalized for catalysts with a greater number of surface reactions by similarly adding more fitting steps as was done for Sn (**Section S1.11**).

Resource Availability

Lead Contact

Inquiries regarding the data and code associated with this paper be directed to Prof. Alexis T. Bell (alexbell@berkeley.edu).

Materials Availability

This study did not generate new materials.

Data and Code Availability

All COMSOL and MATLAB code employed in this study are available on Zenodo (DOI: 10.5281/zenodo.7903605). All code is available for use through the MIT License (<https://opensource.org/license/mit/>). The digitized polarization and partial current density data for all Ag and Sn electrocatalysts fit in this study are openly available at DOI: 10.5281/zenodo.7866274.

Acknowledgements

This material is based on work performed within the Liquid Sunlight Alliance, which is supported by the U.S. Department of Energy, Office of Science, Office of Basic Energy Sciences, Fuels from Sunlight Hub under Award Number DE-SC0021266. JCB would like to acknowledge support from the National Defense Science and Engineering Graduate Fellowship (NDSEG) supported by the Army Research Office (ARO). The authors would also like to acknowledge helpful discussions with Joy Zeng that helped guide the direction of the study.

Author Contributions

JCB developed the model physics and COMSOL continuum model of CO₂R on Ag and Sn used in the study. KRMC and AML developed the utilized covariance matrix adaptation MATLAB code applied to fit kinetic parameters. KRMC linked the COMSOL and MATLAB codes to fit kinetic and transport parameters in the continuum model. JCB and LMP developed the sensitivity analysis for the CO₂R model. KM, AZW, and ATB provided guidance and direction for the project. KRMC and JCB prepared the original draft of the manuscript. All authors engaged in reviewing and editing the manuscript.

Declaration of Interests

The authors declare no competing interests.

Inclusion and Diversity

One or more of the authors of this paper self-identifies as an underrepresented ethnic minority in their field or research of within their geographical location. One or more of the authors of this paper self-identifies as a gender minority within their field of research.

Figure Legends

Figure 1: Traditional Tafel analysis possesses unquantifiable uncertainty that is addressable using a coupled continuum modeling, covariance matrix adaptation approach. Schematic of **(top)** traditional method of processing electrochemical data via Tafel analysis and its associated, unquantifiable human error, and **(bottom)** proposed robust kinetic fitting approach which uses detailed physical models inform

data analysis tools to obtain kinetic parameters with quantifiable uncertainty.

Figure 2: Mass transport limits the applicability of traditional Tafel analysis. Accuracy of Tafel analysis under varying mass-transport regimes with a constant CO Tafel slope. Effect of (a) L_{BL} and (b) i_{0,H_2} on CO Tafel analysis. Solid lines represent simulations where all parameters are fixed except for (a) L_{BL} or (b) i_{0,H_2} . In (a) and (b) dashed lines represent linear regression fits from traditional Tafel analysis (see **Section S1.13**) (Tafel region in blue, and mass transport region in green). (c) Convergence of apparent Tafel slope to actual Tafel slope value as L_{BL} approaches zero. (d) Impact of competing HCOOH reaction on apparent Tafel slope. In (c) and (d) dashed lines represent the value of the Tafel slope as defined in the continuum model as representative of the intrinsic COER kinetics.

Figure 3: CMA-ES fit kinetic parameters are broadly distributed across literature. Probability distribution functions (PDF) (histogram) and kernel density estimates (KDEs) (solid lines) of fit parameters across literature for (a) α_{CO} , (b) $\log_{10}(i_{0,CO})$, (c) α_{H_2} , and (d) $\log_{10}(i_{0,H_2})$. The PDF depicts a histogram of the fitted parameters that has been scaled such that the integrated total of the bars adds to unity. The KDE represents a smoothed version of the PDF in which each bar is assigned a scaled basis function and these basis functions are superimposed to generate the smooth curve. Red dashed lines represent so-called “cardinal values” of the transfer coefficient as determined by analysis shown in **Equation S62**.

Figure 4: Fit exchange current density and transfer coefficient exhibit an apparent compensation phenomenon. Correlation plots for the fit cathodic transfer coefficients and the logarithm of the fit exchange current densities of (a) CO, and (b) H₂. The R² values for these fits are 0.75 and 0.89, respectively.

Figure 5: The continuum, CMA-ES method is extendable to other CO₂ reduction catalysts. Probability distribution functions (PDF) (histogram) and kernel density estimates (KDEs) (solid lines) of the fit (a) α_{CO} , (b) $\log_{10}(i_{0,CO})$, (c) α_{H_2} , (d) $\log_{10}(i_{0,H_2})$, (e) $\alpha_{HCOO^{-i}}$, (f) $\log_{10}(\dot{i})$ for CO₂R on over a Sn catalyst. The PDF depicts a histogram of the fitted parameters that has been scaled such that the integrated total of the bars adds to unity. The KDE represents a smoothed version of the PDF in which each bar is assigned a scaled basis function and these basis functions are superimposed to generate the smooth curve. Red dashed lines represent “cardinal values” of the transfer coefficient as determined by analysis shown in **Equation S62**.

Figure 6: Standard electrochemical compression cell and corresponding physical model. Schematic representation (a) a typical experimental set up, and (b) the corresponding modeled domain for the boundary layer model.

Figure 7: Schematic process of a typical evolution process in CMA-ES for a two-parameter optimization. In the first generation (Generation 1), the CMA-ES creates a generation of points with values of the parameters assigned by an initial Gaussian distribution with a mean at the center of given elliptical bounds and the radii of the ellipse determined by the standard deviations of the distribution (red-dashed lines). CMA-ES ranks the points in terms of how close they are to minimizing the objective function (white locus of the plots) and moves the distribution in the direction of the points with the best ranking regarding objective minimization. In the following generations, the (Generations 2-5) this process is repeated and continues. As the points move closer to the global minimum, the CMA-ES begins to shrink the standard deviation and converge upon the global minimum. The process stops (Generation 6) when the standard deviation of the points reaches a specified, small value, indicating that the generated points all converge upon the global minima.

Figure 8: Process diagram depicting the inputs, outputs, and steps taken to extract kinetic parameters from a given set of experiments using the developed method. (a) Extraction of experimental Tafel data. (b) Shifting of Tafel data to standard conditions. (c) (Top to bottom) Fixing of H₂ current density in COMSOL simulation, fitting CO kinetic parameters with CMA-ES, and quantifying uncertainty. (d) (Top to bottom) Using fit CO kinetics from (c) in the COMSOL model and running CMA-ES to fit H₂ kinetic parameters and extract uncertainty. In panels (c) and (d), $i_{0,k,MT}$ represents the product of the traditional $i_{0,k}$ and the mass-transport activity terms in the Tafel expression shown in Equations (6) and (7).

References

1. Blanco, D.E., and Modestino, M.A. (2019). Organic Electrosynthesis for Sustainable Chemical Manufacturing. *Trends Chem.* *1*, 8–10.
2. De Luna, P., Hahn, C., Higgins, D., Jaffer, S.A., Jaramillo, T.F., and Sargent, E.H. (2019). What Would It Take for Renewably Powered Electrosynthesis to Displace Petrochemical Processes? *Science* (80-.). *364*.
3. Bui, J.C., Lees, E.W., Pant, L.M., Zenyuk, I. V., Bell, A.T., and Weber, A.Z. (2022). Continuum modeling of porous electrodes for electrochemical synthesis. *Chem. Rev.* *122*, 11022–11084.
4. Levi, P., Vass, T., Mandova, H., and Gouy, A. (2018). Chemicals — Analysis (International Energy Agency).
5. Goldman, M., Lees, E.W., Prieto, P.L., Mowbray, B.A.W., Weekes, D.M., Reyes, A., Li, T., Salvatore, D.A., Smith, W.A., and Berlinguette, C.P. (2021). Electrochemical Reactors. In *Carbon Dioxide Electrochemistry: Homogeneous and Heterogeneous Catalysis* (The Royal Society of Chemistry), pp. 408–432.
6. Bui, J.C., Kim, C., King, A.J., Romiluyi, O., Kusoglu, A., Weber, A.Z., and Bell, A.T. (2022). Engineering Catalyst–Electrolyte Microenvironments to Optimize the Activity and Selectivity for the Electrochemical Reduction of CO₂ on Cu and Ag . *Acc. Chem. Res.*
7. Garg, S., Li, M., Weber, A.Z., Ge, L., Li, L., Rudolph, V., Wang, G., and Rufford, T.E. (2020).

- Advances and challenges in electrochemical CO₂ reduction processes: An engineering and design perspective looking beyond new catalyst materials. *J. Mater. Chem. A* **8**, 1511–1544.
8. Nitopi, S., Bertheussen, E., Scott, S.B., Liu, X., Engstfeld, A.K., Horch, S., Seger, B., Stephens, I.E.L., Chan, K., Hahn, C., et al. (2019). Progress and Perspectives of Electrochemical CO₂ Reduction on Copper in Aqueous Electrolyte. *Chem. Rev.* **119**, 7610–7672.
 9. Newman, J., and Thomas-Alyea, K.E. (2004). *Electrochemical Systems* 3rd ed. (John Wiley and Sons, Inc.).
 10. Limaye, A., Zeng, J.S., Willard, A., and Manthiram, K. (2020). Bayesian Data Analysis Reveals No Preference for Cardinal Tafel Slopes in CO₂ Reduction Electrocatalysis.
 11. Shinagawa, T., Garcia-Esparza, A.T., and Takanabe, K. (2015). Insight on Tafel slopes from a microkinetic analysis of aqueous electrocatalysis for energy conversion. *Sci. Rep.* **5**, 1–21.
 12. Dunwell, M., Luc, W., Yan, Y., Jiao, F., and Xu, B. (2018). Understanding Surface-Mediated Electrochemical Reactions: CO₂ Reduction and beyond. *ACS Catal.* **8**, 8121–8129.
 13. Bockris, J.O., and Nagy, Z. (1973). Symmetry Factor and Transfer Coefficient: A Source of Confusion in Electrode Kinetics. *J. Chem. Ed.* **50**, 839–843.
 14. Weng, L.C., Bell, A.T., and Weber, A.Z. (2018). Modeling gas-diffusion electrodes for CO₂ reduction. *Phys. Chem. Chem. Phys.* **20**, 16973–16984.
 15. Clark, E.L., Resasco, J., Landers, A., Lin, J., Chung, L.T., Walton, A., Hahn, C., Jaramillo, T.F., and Bell, A.T. (2018). Standards and Protocols for Data Acquisition and Reporting for Studies of the Electrochemical Reduction of Carbon Dioxide. *ACS Catal.* **8**, 6560–6570.
 16. Agbo, P., and Danilovic, N. (2019). An Algorithm for the Extraction of Tafel Slopes. *J. Phys. Chem. C* **123**, 30252–30264.

17. Khadke, P., Tichter, T., Boettcher, T., Muench, F., Ensinger, W., and Roth, C. (2021). A simple and effective method for the accurate extraction of kinetic parameters using differential Tafel plots. *Sci. Rep.* *11*, 8974.
18. Rabinowitz, J.A., and Kanan, M.W. (2020). The future of low-temperature carbon dioxide electrolysis depends on solving one basic problem. *Nat. Commun.*, 10–12.
19. Zhang, Z., Melo, L., Jansonius, R.P., Habibzadeh, F., Grant, E.R., and Berlinguette, C.P. (2020). pH Matters When Reducing CO₂ in an Electrochemical Flow Cell. *ACS Energy Lett.* *5*, 3101–3107.
20. Liu, X., Schlexer, P., Xiao, J., Ji, Y., Wang, L., Sandberg, R.B., Tang, M., Brown, K.S., Peng, H., Ringe, S., et al. (2019). pH effects on the electrochemical reduction of CO₍₂₎ towards C₂ products on stepped copper. *Nat Commun* *10*, 32.
21. Hashiba, H., Weng, L.C., Chen, Y., Sato, H.K., Yotsuhashi, S., Xiang, C., and Weber, A.Z. (2018). Effects of electrolyte buffer capacity on surface reactant species and the reaction rate of CO₂ in Electrochemical CO₂ reduction. *J. Phys. Chem. C* *122*, 3719–3726.
22. Yang, K., Kas, R., and Smith, W.A. (2019). In Situ Infrared Spectroscopy Reveals Persistent Alkalinity near Electrode Surfaces during CO₂ Electroreduction. *J. Am. Chem. Soc.* *141*.
23. Koshy, D.M., Akhade, S.A., Shugar, A., Abiose, K., Shi, J., Liang, S., Oakdale, J.S., Weitzner, S.E., Varley, J.B., Duoss, E.B., et al. (2021). Chemical Modifications of Ag Catalyst Surfaces with Imidazolium Ionomers Modulate H₂ Evolution Rates during Electrochemical CO₂ Reduction. *J. Am. Chem. Soc.* *143*, 14712–14725.
24. Thevenon, A., Rosas-Hernández, A., Fontani Herreros, A.M., Agapie, T., and Peters, J.C. (2021). Dramatic HER Suppression on Ag Electrodes via Molecular Films for Highly Selective CO₂ to CO

- Reduction. *ACS Catal.* *11*, 4530–4537.
25. Ma, M., Trzeźniewski, B.J., Xie, J., and Smith, W.A. (2016). Selective and Efficient Reduction of Carbon Dioxide to Carbon Monoxide on Oxide-Derived Nanostructured Silver Electrocatalysts. *Angew. Chemie - Int. Ed.* *55*, 9748–9752.
 26. Clark, E.L., Ringe, S., Tang, M., Walton, A., Hahn, C., Jaramillo, T.F., Chan, K., and Bell, A.T. (2019). Influence of Atomic Surface Structure on the Activity of Ag for the Electrochemical Reduction of CO₂ to CO. *ACS Catal.* *9*, 4006–4014.
 27. Peng, X., Karakalos, S.G., and Mustain, W.E. (2018). Preferentially Oriented Ag Nanocrystals with Extremely High Activity and Faradaic Efficiency for CO₂ Electrochemical Reduction to CO. *ACS Appl. Mater. Interfaces* *10*, 1734–1742.
 28. Ma, M., Liu, K., Shen, J., Kas, R., and Smith, W.A. (2018). In Situ Fabrication and Reactivation of Highly Selective and Stable Ag Catalysts for Electrochemical CO₂ Conversion. *ACS Energy Lett.* *3*, 1301–1306.
 29. Hatsukade, T., Kuhl, K.P., Cave, E.R., Abram, D.N., and Jaramillo, T.F. (2014). Insights into the electrocatalytic reduction of CO₂ on metallic silver surfaces. *Phys. Chem. Chem. Phys.* *16*, 13814–13819.
 30. Kim, C., Jeon, H.S., Eom, T., Jee, M.S., Kim, H., Friend, C.M., Min, B.K., and Hwang, Y.J. (2015). Achieving Selective and Efficient Electrocatalytic Activity for CO₂ Reduction Using Immobilized Silver Nanoparticles. *J. Am. Chem. Soc.* *137*, 13844–13850.
 31. Yuan, X., Wu, Y., Jiang, B., Wu, Z., Tao, Z., Lu, X., Liu, J., Qian, T., Lin, H., and Zhang, Q. (2020). Interface Engineering of Silver-Based Heterostructures for CO₂ Reduction Reaction. *ACS Appl. Mater. Interfaces* *12*, 56642–56649.

32. Nakamura, M., Sato, N., Hoshi, N., and Sakata, O. (2011). Outer Helmholtz Plane of the Electrical Double Layer Formed at the Solid Electrode–Liquid Interface. *ChemPhysChem* *12*, 1430–1434.
33. Bui, J.C., Kim, C., Weber, A.Z., and Bell, A.T. (2021). Dynamic Boundary Layer Simulation of Pulsed CO₂ Electrolysis on a Copper Catalyst. *ACS Energy Lett.* *6*, 1181–1188.
34. Delacourt, C., and Newman, J. (2010). Mathematical Modeling of CO₂ Reduction to CO in Aqueous Electrolytes II. Study of an Electrolysis Cell Making Syngas (CO + H₂) from CO₂ and H₂O Reduction at Room Temperature. *J. Electrochem. Soc.* *157*, B1911–B1926.
35. Vos, R.E., and Koper, M.T.M. (2022). The Effect of Temperature on the Cation-Promoted Electrochemical CO₂ Reduction on Gold. *ChemElectroChem* *9*, 1–11.
36. Wuttig, A., Yaguchi, M., Motobayashi, K., Osawa, M., and Surendranath, Y. (2016). Inhibited proton transfer enhances Au-catalyzed CO₂-to-fuels selectivity. *Proc. Natl. Acad. Sci. U. S. A.* *113*, E4585–E4593.
37. Akimoto, Y., Auger, A., Hansen, N., Auger, A., Hansen, N., Auger, A., Hansen, N., Auger, A., and Hansen, N. (2015). Tutorial: Evolution Strategies and CMA-ES (Covariance Matrix Adaptation) Continuous Domain Search / Optimization Continuous Domain Search / Optimization Objective Function Properties Goal. *Proc. 2015 Annu. Conf. Genet. Evol. Comput.*, 333–355.
38. Williams, K., Corbin, N., Zeng, J., Lazouski, N., Yang, D.T., and Manthiram, K. (2019). Protecting effect of mass transport during electrochemical reduction of oxygenated carbon dioxide feedstocks. *Sustain. Energy Fuels* *3*, 1225–1232.
39. Higgins, D., Hahn, C., Xiang, C., Jaramillo, T.F., and Weber, A.Z. (2019). Gas-Diffusion Electrodes for Carbon Dioxide Reduction: A New Paradigm. *ACS Energy Lett.* *4*, 317–324.

40. Jang, J., Rüscher, M., Winzely, M., and Morales-Guio, C.G. (2022). Gastight rotating cylinder electrode: Toward decoupling mass transport and intrinsic kinetics in electrocatalysis. *AIChE J.* *68*.
41. Richard, D., Tom, M., Jang, J., Yun, S., Christofides, P.D., and Morales-Guio, C. (2022). Quantifying Transport and Reaction Electrocatalytic Processes in a Gastight Rotating Cylinder Electrode Reactor Via Integration of Computational Fluid Dynamics Modeling and Experiments. *SSRN Electron. J.* *440*.
42. Nguyen, D.L.T., Nguyen, T.M., Lee, S.Y., Kim, J., Kim, S.Y., Le, Q. Van, Varma, R.S., and Hwang, Y.J. (2022). Electrochemical conversion of CO₂ to value-added chemicals over bimetallic Pd-based nanostructures: Recent progress and emerging trends. *Environ. Res.* *211*, 113116.
43. Ge, H., Gu, Z., Han, P., Shen, H., Al-Enizi, A.M., Zhang, L., and Zheng, G. (2018). Mesoporous tin oxide for electrocatalytic CO₂ reduction. *J. Colloid Interface Sci.* *531*, 564–569.
44. Liu, G., Li, Z., Shi, J., Sun, K., Ji, Y., Wang, Z., Qiu, Y., Liu, Y., Wang, Z., and Hu, P.A. (2020). Black reduced porous SnO₂ nanosheets for CO₂ electroreduction with high formate selectivity and low overpotential. *Appl. Catal. B Environ.* *260*, 118134.
45. Daiyan, R., Lovell, E.C., Bedford, N.M., Saputera, W.H., Wu, K.H., Lim, S., Horlyck, J., Ng, Y.H., Lu, X., and Amal, R. (2019). Modulating Activity through Defect Engineering of Tin Oxides for Electrochemical CO₂ Reduction. *Adv. Sci.* *6*, 1–9.
46. Corva, M., Blanc, N., Bondue, C.J., and Tschulik, K. (2022). Differential Tafel Analysis: A Quick and Robust Tool to Inspect and Benchmark Charge Transfer in Electrocatalysis. *ACS Catal.* *12*, 13805–13812.
47. Singh, M.R., Goodpaster, J.D., Weber, A.Z., Head-Gordon, M., and Bell, A.T. (2017).

- Mechanistic insights into electrochemical reduction of CO₂ over Ag using density functional theory and transport models. *Proc. Natl. Acad. Sci. U. S. A.* *114*, E8812–E8821.
48. van der Heijden, O., Park, S., Eggebeen, J.J.J., and Koper, M.T.M. (2023). Non-Kinetic Effects Convolute Activity and Tafel Analysis for the Alkaline Oxygen Evolution Reaction on NiFeOOH Electrocatalysts. *Angew. Chemie - Int. Ed.* *62*, 1–9.
 49. Bard, A.J., and Faulkner, L.R. (2001). *Electrochemical Methods: Fundamentals and Applications* 2nd ed. (Wiley).
 50. Hansen, H.A., Varley, J.B., Peterson, A.A., and Nørskov, J.K. (2013). Understanding trends in the electrocatalytic activity of metals and enzymes for CO₂ reduction to CO. *J. Phys. Chem. Lett.* *4*, 388–392.
 51. Liu, X.Y., Schlexer, P., Xiao, J.P., Ji, Y.F., Wang, L., Sandberg, R.B., Tang, M., Brown, K.S., Peng, H.J., Ringe, S., et al. (2019). pH effects on the electrochemical reduction of CO₍₂₎ towards C₂ products on stepped copper. *Nat. Commun.* *10*.
 52. Li, J., Stenlid, J.H., Ludwig, T., Lamoureux, P.S., and Abild-Pedersen, F. (2021). Modeling Potential-Dependent Electrochemical Activation Barriers: Revisiting the Alkaline Hydrogen Evolution Reaction. *J. Am. Chem. Soc.* *143*, 19341–19355.
 53. Gauthier, J.A., Stenlid, J.H., Abild-Pedersen, F., Head-Gordon, M., and Bell, A.T. (2021). The Role of Roughening to Enhance Selectivity to C₂+ Products during CO₂ Electroreduction on Copper. *Acs Energy Lett.*, 3252–3260.
 54. Motagamwala, A.H., and Dumesic, J.A. (2020). Microkinetic Modeling: A Tool for Rational Catalyst Design. *Chem. Rev.*
 55. Vetter, K.J. (1961). *Elektrochemische Kinetik* (Springer).

56. Resasco, J., Abild-Pedersen, F., Hahn, C., Bao, Z., Koper, M.T.M., and Jaramillo, T.F. (2022). Enhancing the connection between computation and experiments in electrocatalysis. *Nat. Catal.* *5*, 374–381.
57. Bond, G.C., Keane, M.A., Kral, H., and Lercher, J.A. (2000). Compensation Phenomena in Heterogeneous Catalysis: General Principles and a Possible Explanation. *Catal. Rev. - Sci. Eng.* *42*, 323–383.
58. Bligaard, T., Honkala, K., Logadottir, A., Nørskov, J.K., Dahl, S., and Jacobsen, C.J.H. (2003). On the compensation effect in heterogeneous catalysis. *J. Phys. Chem. B* *107*, 9325–9331.
59. Roduner, E. (2014). Understanding catalysis. *Chem. Soc. Rev.* *43*, 8226–8239.
60. Barrie, P.J. (2012). The mathematical origins of the kinetic compensation effect: 1. the effect of random experimental errors. *Phys. Chem. Chem. Phys.* *14*, 318–326.
61. Akbashev, A.R. (2022). Electrocatalysis Goes Nuts. *ACS Catal.* *12*, 4296–4301.
62. Watkins, N.B., Schiffer, Z.J., Lai, Y., Musgrave Iii, C.B., Atwater, H.A., Iii, W.A.G., Agapie, T., Peters, J., and Gregoire, J.M. (2023). Hydrodynamics Determine Tafel Slopes in Electrochemical CO₂ Reduction on Copper.
63. Yang, D.T., Zhu, M., Schiffer, Z.J., Williams, K., Song, X., Liu, X., and Manthiram, K. (2019). Direct Electrochemical Carboxylation of Benzylic C-N Bonds with Carbon Dioxide. *ACS Catal.* *9*, 4699–4705.
64. Chung, M., Jin, K., Zeng, J.S., Ton, T.N., and Manthiram, K. (2022). Tuning Single-Atom Dopants on Manganese Oxide for Selective Electrocatalytic Cyclooctene Epoxidation. *J. Am. Chem. Soc.* *144*, 17416–17422.
65. Lazouski, N., Chung, M., Williams, K., Gala, M.L., and Manthiram, K. (2020). Non-aqueous gas

diffusion electrodes for rapid ammonia synthesis from nitrogen and water-splitting-derived hydrogen. *Nat. Catal.* 3.